Understanding and modeling glitch effects in ISOCAM and other future space telescopes

Arnaud J. Claret[a] and Koryo Okumura[b]

[a]CEA-Saclay, Service d'Astrophysique, F-91191, Gif-sur-Yvette, France
[b]CNRS-URA2052, France

ABSTRACT

One of the main limitations to the sensitivity of photodetector operated in space comes from responsivity variations and glitches caused by the impacts of charged particles. An international glitch working group (GWG) was created in order to centralize information about these phenomena and prepare future space experiments. Results about the infrared camera ISOCAM on-board the Infrared Space Observatory (ISO) are presented here:

- The predicted glitch rate has been analytically evaluated and compared to in-flight measurements.
- The study of temporal and spatial properties of glitches has led to a classification into 3 distinct families. These families are related to the linear energy transfer (LET) of charged particles interacting with the detectors.
- Removal methods of glitch effects are briefly addressed.
- Monte-Carlo simulations of radiation effects have been made. Glitch rates, spatial and energetic properties of glitches have been computed. Monte-Carlo results are compared with measured values.
- Perspectives and current studies for HERSCHEL are discussed.

Keywords: Space telescope, ISO, radiation effects, Monte-Carlo methods

1. INTRODUCTION

During the first ISO detector workshop (Madrid, 1998), a number of detailed technical reports of the performance of ISO detectors were presented, along with more general discussions on glitch effects, transient effects and future detector strategies, particularly in view of the upcoming HERSCHEL (previously named FIRST) and NGST (Next Generation Space Telescope) missions. The so-called glitch phenomenon is the result of an energy deposit from charged particles in detectors operating in space. This phenomenon requires detailed knowledge of the cosmic ray environment, trapped electron and proton fluxes, and other space environmental parameters. The GWG has been created in order to provide information on the radiation environment of the ISO orbit during the mission (1995-1998). Analysis of glitch effects in the four ISO[1] instruments (ISOCAM camera, ISOPHOT photometer, ISOLWS long wave spectrometer, and ISOSWS short wave spectrometer) is indeed of great interest to prepare future space experiments, such as HERSCHEL or NGST. The final version of the GWG final report[2] about ISO glitches is now available.

After a brief description of the ISOCAM radiation environment (Sect. 2.1), main characteristics of radiation effects on ISOCAM are described and explained (Sect. 2.2, Sect. 2.3, Sect. 2.4). Removal methods of glitch effects in data are briefly adressed in Sect. 2.5. Monte-Carlo simulations are described in Sect. 3.1 and Sect. 3.2. Results of simulations are given in Sect. 3.3 and discussed in Sect. 3.4. Preliminary studies and perspectives for the next infrared space experiment HERSCHEL are presented in Sect. 4.

Further author information: (Send correspondence to A.J.C.)
A.J.C.: E-mail: aclaret@cea.fr, Telephone: +33 1 6908 6130
K.O.: E-mail: koryo.okumura@cea.fr, Telephone: +33 1 6908 6299, Address: CEA-Saclay, Service d'Astrophysique, F-91191, Gif-sur-Yvette, France

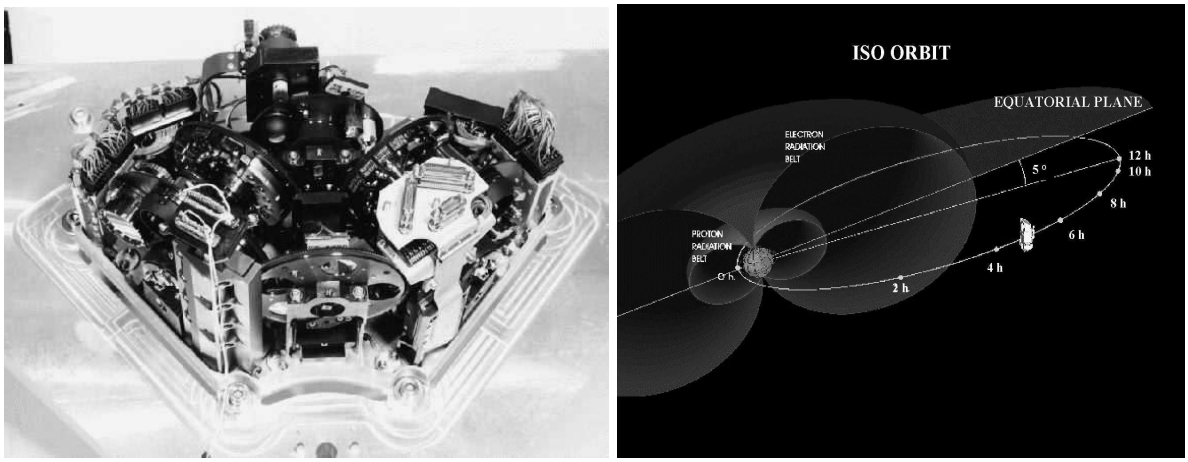

Figure 1. Left image shows the focal plane unit of the ISOCAM flight model. The optical beam enters in the camera through the entrance wheel (foreground) and can be directed to the short (SW) or the long wavelength (LW) channel by field mirrors fixed on the selection wheel (background). Each channel includes a filter wheel and a selection wheel. Right image displays the main parameters of ISO orbit: apogee altitude was 70,550 km, perigee altitude was 1,000 km, period was 24 hours and inclination with respect to the equatorial plan was 5°.

2. UNDERSTANDING GLITCH EFFECTS IN ISOCAM

2.1. ISOCAM camera and ISO orbit

The infrared camera ISOCAM was operated at very low temperature on board ISO from November 1995 until April 1998. Since all details about the ISOCAM camera[3] can be found elsewhere, only the main characteristics relevant for Monte-Carlo simulations are presented here. ISOCAM was designed to operate in the 2.5-17 μm range with two detectors of 32×32 pixels at 2.4 K thanks to passive helium cooling (Fig. 1):

- a long wave (LW) detector using a SiGa substrate (100 μm pitch and 500 μm thickness) with a Direct Readout Output circuit, for 4-17 μm wavelengths,
- a short wave (SW) detector using a InSb substrate (thickness $\leq$10 μm) and a Charge Injection Device readout method, for 2.5-5 μm wavelengths.

The ISO telescope was operated in a highly elliptical 24-hour orbit (Fig. 1). The lowest part of the orbit lied inside the Earth's van Allen belts of trapped electrons and protons. Inside the belts, ISO's detectors were scientifically unusable due to effects caused by proton and electron impacts. Outside the radiation belts ($\approx$ 16 hours), the spacecraft was directly exposed to galactic cosmic rays (GCRs). GCRs are composed of 87% protons, 12% alphas, and 1% heavier nuclei. The differential spectrum of GCRs is roughly peaked at 500 MeV/n. Occasional solar particle events produced additional protons and heavier nuclei.

2.2. Glitch rate

Along the ISO orbit, the perturbations came from GCRs and trapped particles in the van Allen belts. Their fluxes are defined within a factor 2, depending on the solar activity. Since the spacecraft body was equivalent to 2.5 cm of aluminum, only particles with energy greater than 80 MeV/n could traverse this shield. Spectra of galactic protons and alphas were computed by Spacerad* (version 4). They were normalized with measurements of protons made by KET (Kinetic Electron Telescope) when it was close to the ecliptic plane. The integral spectra above 80 MeV/n were compared to the KET spectra and the normalization factors deduced. The proton and alpha spectra produced by Spacerad were then multiplied by these normalization factors. Corresponding

*Space Radiation Version 4.0 is a commercial code from Space Radiation Associates, Eugene, Oregon, 1996.

fluxes are 0.39 cm^{-2} sr^{-1} s^{-1} and 0.032 cm^{-2} sr^{-1} s^{-1} respectively for galactic protons and alphas. Neglecting the flux of heavier nuclei, this leads to $\Phi_{GCRs} = 0.422$ cm^{-2} sr^{-1} s^{-1}.

Let Φ be the particle flux per cm^{-2} sr^{-1} s^{-1}, the incoming flux passing through the surface unit dS is:

$$\phi = \Phi \int_0^{\frac{\pi}{2}} 2\pi sin\theta dS\ cos\theta d\theta = \pi \Phi dS$$

If the detector is approximated by a rectangle parallelepiped of dimensions A, B and C, the incoming flux through all its faces[4] is $\phi_{directs\ impacts} \approx \pi\ \Phi_{GCRs} \times\ 2(AB + BC + AC)$, leading to:

$$\begin{aligned} \phi_{directs\ impacts} &= 0.844 \times \Phi_{GCRs} \approx 0.36\ s^{-1} \text{ for LW detector (A = B = 0.32 cm and C = 0.05 cm)} \\ &= 0.645 \times \Phi_{GCRs} \approx 0.27\ s^{-1} \text{ for SW detector (A = B = 0.32 cm and C = 0.0005 cm)} \end{aligned}$$

Analytic calculation[4] shows that primary particles passing through the surrounding materials also produce $\approx 80\%$ of additional events, by either nuclear reactions or δ-ray emissions (electrons emitted along the track of particles with subrelativistic velocity). δ-ray emission is proportional to Z^2 of the incoming particle.

In addition to these external particles, the anti-reflection coating of lenses contains traces of radioactive ^{232}Th, which generates a flux of low energy (4 MeV) α-particles. The flux of these α-particle depends on the solid angle of the lens viewed from the array (0.35 s^{-1} from the 12 arcsec/pixel lens, 0.16 s^{-1} from the 6 arcsec/pixel lens, 0.02 s^{-1} from the 3 arcsec/pixel lens, 0.002 s^{-1} from the 1.5 arcsec/pixel lens). Fortunately, the 12 arcsec/pixel lens, for which the flux of α-particles is maximum, was quite never used (due to distortion of field of view).

All contribution are summarized in Table 1. Neither the electro-magnetic showers, nor the secondary particles from the body of spacecraft have been taken into account here. These last contributions are more difficult to derive and require Monte-Carlo simulations.

Table 1. Predicted glitch rate for ISOCAM detectors (s^{-1}).

Primary GCRs (protons + alphas)		0.36		
Secondary particles and δ-rays		0.29		
Lens (arcsec/pixel)	1.5	3	6	12
α-particles produced by lenses (^{232}Th)	0.002	0.02	0.16	0.35
TOTAL for LW detector	**0.65**	**0.67**	**0.81**	**1.0**
Primary GCRs (protons + alphas)		0.27		
Secondary particles and δ-rays		0.22		
Lens (arcsec/pixel)	1.5	3	6	12
α-particles produced by lenses (^{232}Th)	0.002	0.02	0.16	0.35
TOTAL for SW detector	**0.49**	**0.51**	**0.65**	**0.84**

2.3. Glitch length

The glitch length can be understood only by geometrical considerations. Considering isotropic incident particles and approximating the detector by a rectangle parallelepiped, the incoming flux through all the faces is merely $\phi_{detector} = \pi\Phi_{GCRs} \times 2(AB + BC + AC)$, where A, B and C are the dimensions of the detector. Similarly, the total flux traversing the set of N pixels of the detector is $\phi_{all\ pixels} = N \times [\pi\Phi_{GCRs} \times 2(ab + bc + ac)]$, where a, b and c are the pixel dimensions. Assuming that the particles follow straight lines in the detector, the average track length $< n >$ in pixel units does not depend on Φ_{GCRs} and is given by:

$$< n > \sim\ \frac{\phi_{all\ pixels}}{\phi_{detector}} = \frac{N \times (ab + bc + ac)}{(AB + BC + AC)}$$

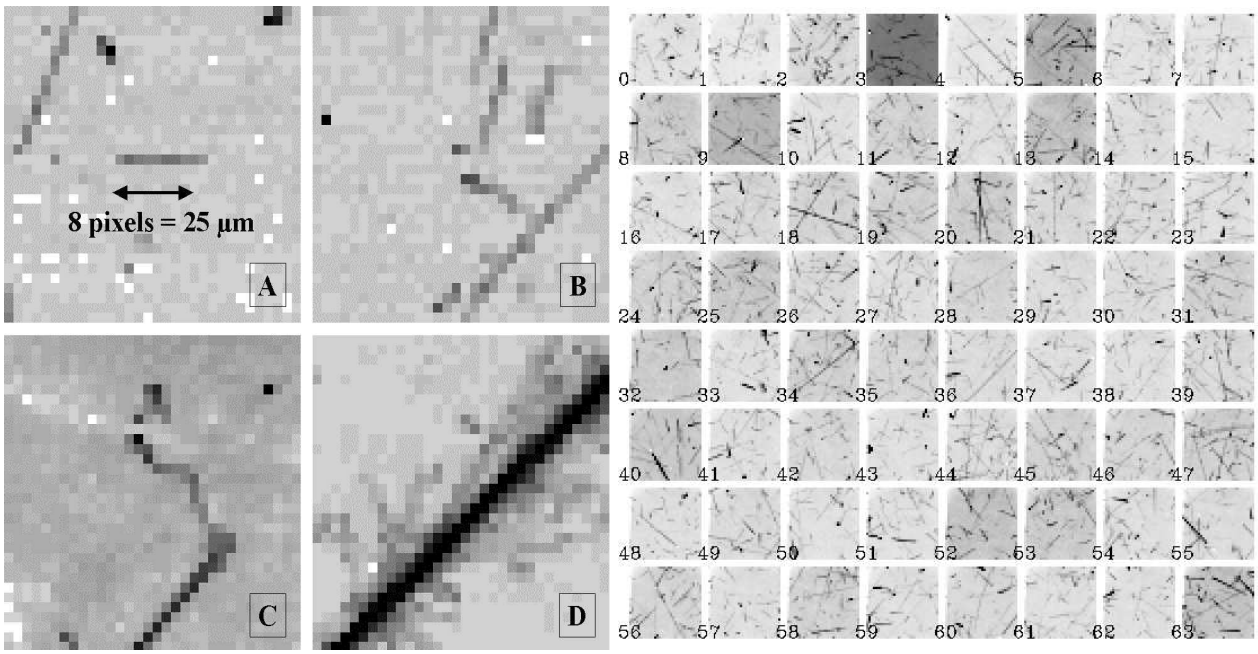

Figure 2. Images of LW detector. There are twice more glitches in 10.08 s images (panel B) than in 5.04 s images (panel A). More precisely, there is ≈ 1 glitch/s in LW images and the average glitch length is 8 pixels. In panel C, a low energy particle has stopped inside the detector (the incoming particle has collided a nucleus of the detector and the faint track might be the result of this recoil nucleus). The track of panel D is interpreted as a nuclear reaction occurring in the detector by high-energy heavy ion passing through the detector. Right panel displays a series of successive LW images degraded by many glitches which occurred during the solar event of November 1997 (the glitch rate has increased by a factor of at least 7, and probably around 10).

Taking the number of pixels (N=1024), the pixel dimensions (a = b = 0.01 cm for both detectors, c = 0.05 cm for LW and c = 0.0005 cm for SW) and the whole detector dimensions (A = B = 0.32 cm for both detectors, C = 0.05 cm for LW and C = 0.0005 cm for SW), the above equation gives:

$$\begin{aligned} < n > &= \text{8.4 pixels per track for LW glitches,} \\ &= \text{0.8 pixels per track for SW glitches.} \end{aligned}$$

Active zone of SW pixels was very thin, so it had a low susceptibility to radiation effects. The LW detector was much thicker, leading to a much higher susceptibility to radiation effects. Longer glitches are obtained when the incidence of incoming particle is close to 0°. On the contrary, particles hitting the detector with a normal incidence produce short glitches (1-2 pixels per glitch, rather than a streak). This is the case for α-particles coming from the radioactive anti-reflection coating of lenses. Fig. 2 shows various example of glitches recorded by the LW detector.

2.4. Glitch profile

Glitches can be divided into three families based on their temporal profile (see Fig. 3). These temporal profiles can be understood by considering the LET of charged particles interacting with the detectors. The associated current can be divided in two components: (a) the primary current instantaneously generated and directly associated with the transport of the carriers (free electron-hole pairs) and (b) the secondary current (exponential decay) corresponding to the dielectric relaxation of the detector. When the LET is small (i.e. when the secondary current is short), the amplitude of the exponential decay is small and the associated decay constant is too rapid

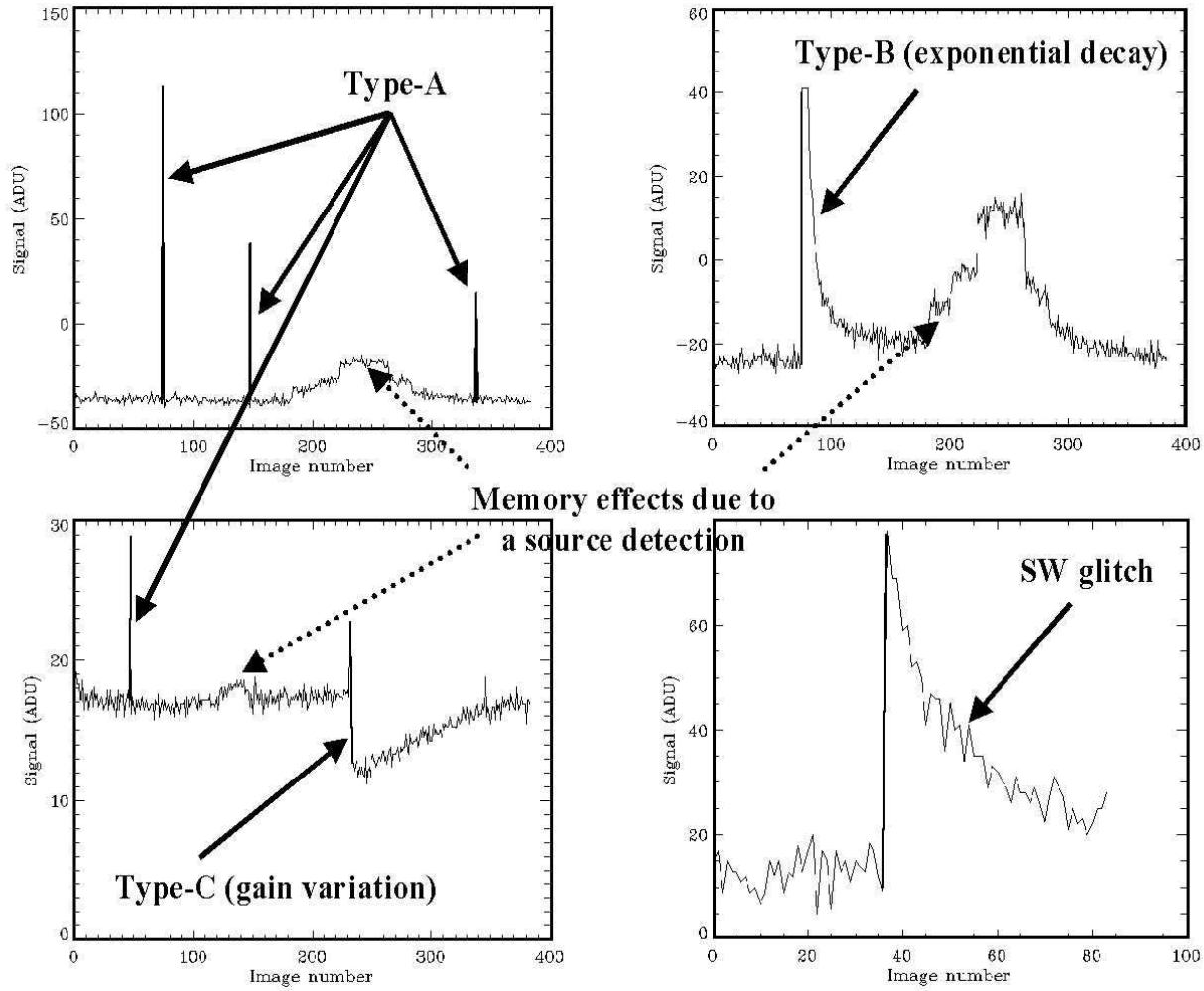

Figure 3. Time profiles of some individual pixels hitted by GCRs. Glitches of LW detector have been divided into three families called Type-A, Type-B and Type-C glitches. The decay time is roughly as short as the rise time for common glitches (Type-A) whereas it is much longer than the rise time and has an exponential profile for fader glitches (Type-B). The detector gain is affected for dipper glitches (Type-C) and the nominal sensitivity is recovered only after several readouts. This gain variation can be misinterpreted as a memory effect by correction algorithms and can thus lead to a false source detection. Note also that Type-C glitches are not necessarily the strongest ones in amplitude. The lower right image shows a glitch of SW detector: they all look like Type-B glitch of LW detector, with a long decay time.

to be observed within the detector integration period. This leads to a Type-A glitch. When the LET is higher (i.e. when the secondary current is longer), the dielectric relaxation of the detector takes a longer time and the exponential decay can be sampled, leading to a Type-B glitch. When the LET is even higher, the detector retains a higher net positive or negative charge after the primary current is over. The electric field[5] can then be modified by this amount of charges, leading to some temporary negative currents, typical of Type-C glitches. The LET depends on the energy of the incident particle and also on its atomic number (proportional to Z^2). We expect that Type-A glitches are induced by galactic protons and electrons, whereas Type-B glitches are induced by light galactic ions. Type-C glitches would be induced by particles providing higher LET such as heavy galactic ions.

2.5. Removal methods

The energy deposit by an incoming particle is spatially localized and it takes a limited period of time for the detector to recover from it. A glitch can thus be detected by using spatial and/or temporal criteria with rather simple algorithms. Nevertheless, in order to have a robust and efficient method, it appeared necessary to use pattern recognition. Due to the limited space, the reader is referred to a previous paper[5] where all glitch removal methods used in the ISOCAM data interactive analysis are described.

3. MODELING GLITCH EFFECTS IN ISOCAM

3.1. Radiation environment

In this paper, we present simulations of particle effects from GCRs (protons and alphas, not heavy ions) and also internal particles (α-particles produced by traces of ^{232}Th contained in the anti-reflecting coating of lenses). Note that there are two significant differences between alphas from GCRs and α-particles from the lens coating. First, alphas from GCRs have an isotropic directional distribution (average glitch length is 8 pixels) whereas α-particles from ^{232}Th hit the detector with a normal incidence (average glitch length is 1-2 pixels). Secondly, alphas from GCRs have enough energy to traverse the detector, whereas α-particles from ^{232}Th are stopped in less than 20μm. So the deposited energy by α-particles from ^{232}Th is higher than for alphas of GCRs in spite of their lower incident energy (see also Table 2 in Sect. 3.3).

Spectra of galactic protons and alphas were computed as indicated in Sect. 2.2. For illustration purpose, the proton spectrum is displayed on Fig. 4. α-particles coming from radioactive coating of lenses have an energy of 4 MeV. Since they have to escape from the lens coating, their spectrum is not strictly mono-energetic when arriving on the detector. But it did not appear necessary to consider a attenuated spectrum for these α-particles.

3.2. Geometrical model

In order to simplify the interpretation, a simple geometry was used for modeling the lens and filter wheels, the detector mounting, and the spacecraft shielding (Fig. 5). The region of charge collection (ie the detector) was modeled as a rectangle parallelepiped. It was divided in 32×32 elementary volumes in order to simulate the pixels of the detector.

3.3. Results

The GEANT[6] Monte-Carlo code (version 3.1) was used to simulate the particle transport of primary particle fluxes. Energy loss by ionisation, δ-ray generation, hadron interactions and multiple scattering have been simulated. GEANT calculated the energy loss following the particle through all interactions in true Monte-Carlo form. Energy deposits have been recorded in a 3-dimensional space (x,y,E) representing respectively the pixel coordinates and the amount of deposited energy. It was thus easy to compute statistics on simulated glitches. Full distributions of interesting parameters (such as deposited energy, glitch length, glitch rate, ...) were then available.

Images of synthetic glitches have been produced (see Fig. 5) and look very similar to real data (see Fig. 2). Contribution of galactic protons and alphas to the glitch rate as a function of the energy of incident particle has been computed (see Fig. 6 for protons). The total glitch rate from GCRs is $\approx 0.88 \pm 0.13$ s^{-1}in very good agreement with the expected values described in Sect. 2.2. Considering that there is 0.36 s^{-1} direct impacts for

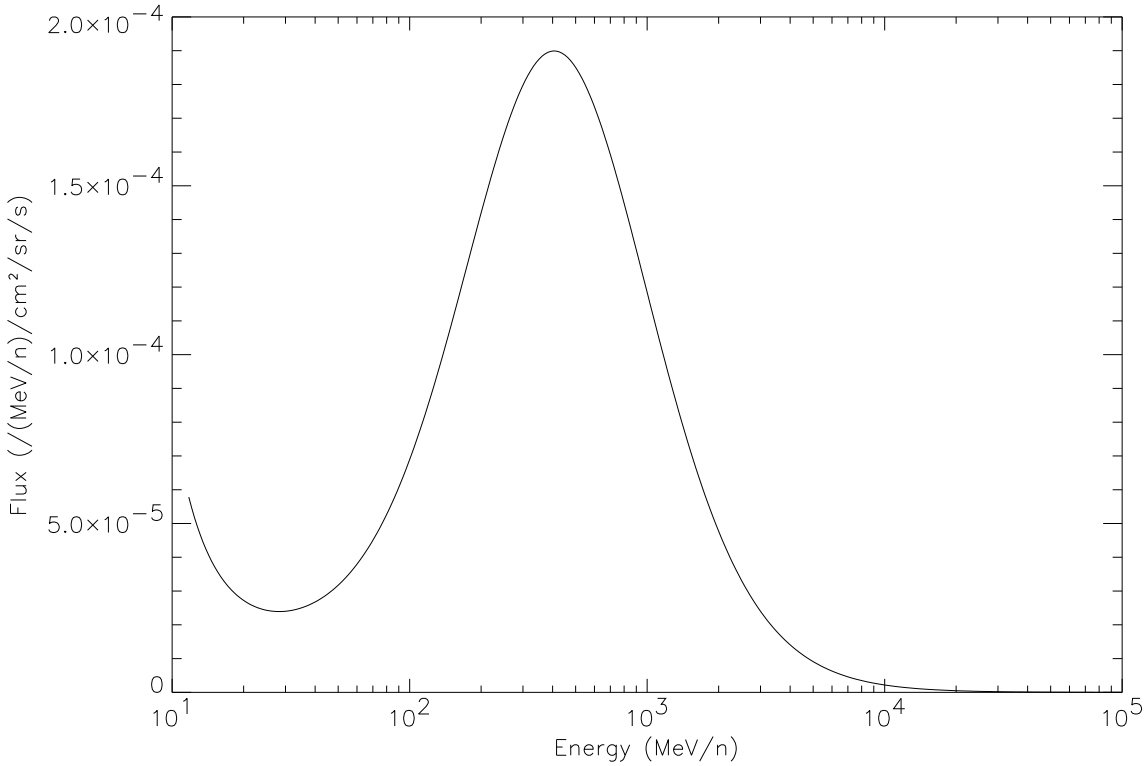

Figure 4. The galactic proton spectrum derived from Spacerad 4 (M=1 solar minimum) and normalized with KET spacecraft data.

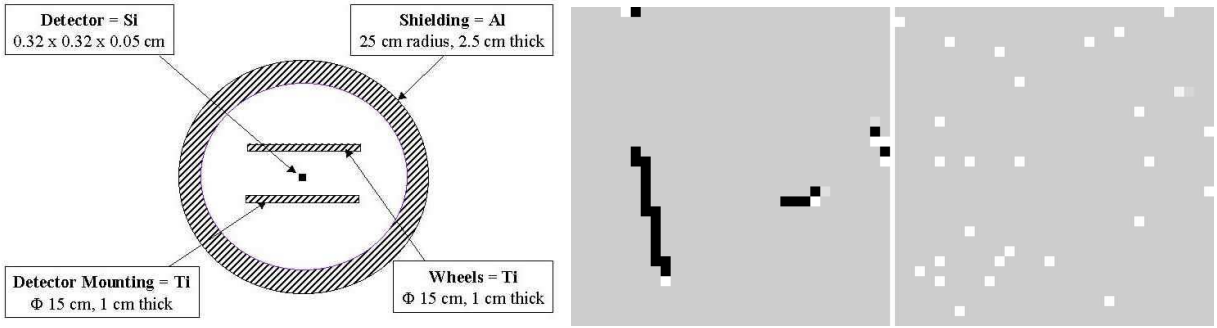

Figure 5. The simple geometrical model of the detector surroundings used in Monte-Carlo simulations and examples of synthetic glitches produced by these simulations. Left image is the contribution of galactic protons with an average energy of 600 MeV for a 5 s integrated LW image. Right image is the contribution of α-particles (4 MeV) produced by the radioactive lens coating (^{232}Th) for a 10 min (not realistic but for illustration purpose) integrated LW image.

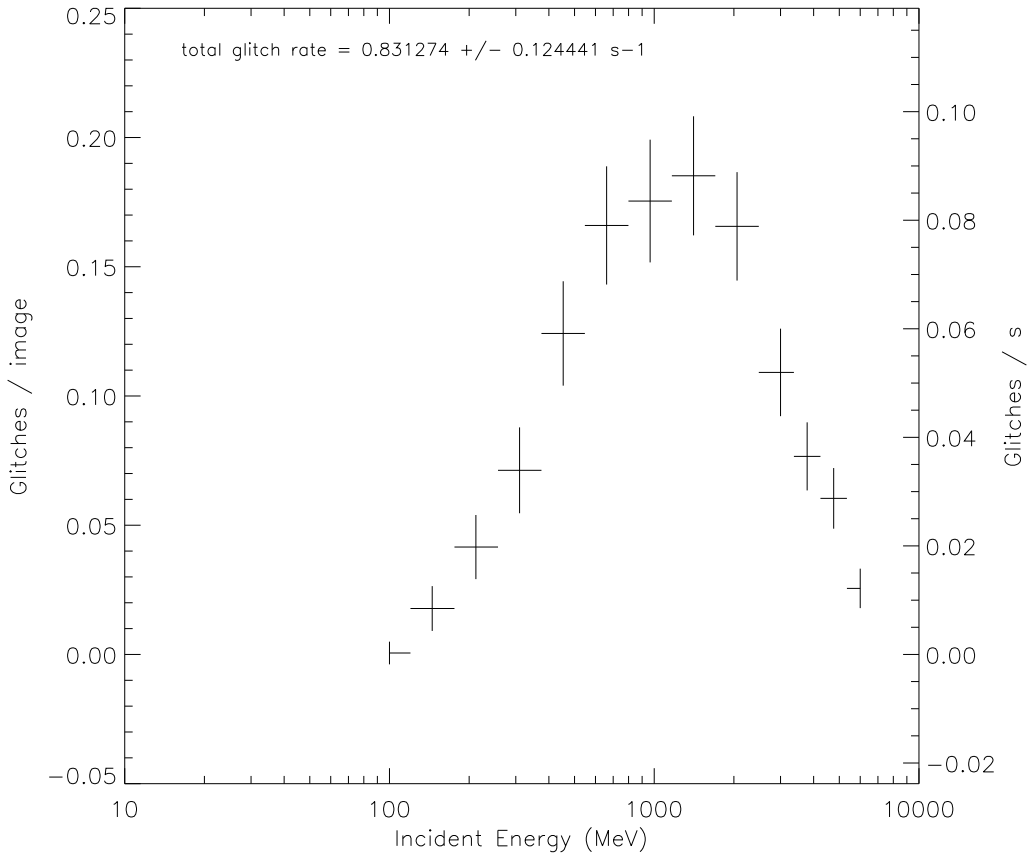

Figure 6. Contribution of galactic protons to the glitch rate as a function of the energy of incident particle, computed by Monte-Carlo simulations. The total (on the whole energy range) glitch rate from galactic proton is 0.83 ± 0.12 s^{-1}. In the same way, the total glitch rate from galactic alphas is found to be 0.045 ± 0.026 s^{-1}. The derived total glitch rate from GCRs (protons + alphas) is $\approx 0.88 \pm 0.13$ s^{-1}.

LW detector (Table 1), this leads to 0.51 s^{-1} for secondary impacts. So the contribution of secondary particles and δ-rays represents $\approx 60\%$ of the direct impacts according to the GEANT code. We have also derived the length and the individual energy deposit for each track (see Fig. 7 for protons).

Monte-Carlo results are summarized in Table 2. Note that the GEANT code was used to simulate only the particle transport, not the radiation impacts on the electronics or the readout circuits. For example, a model the distribution of charge collection[5] over time would be necessary but this was out of the scope of this paper. Nevertheless, such a modelisation would be necessary in order to understand better the phenomenology of Type-C glitches.

Table 2. Summary of Monte-Carlo results (values marked with the asterisk depend on the lens in use).

	Protons of GCRs	Alphas of GCRs	α-particles produced by lenses
Typical incident energy (MeV)	600	2000	4
Energy per glitch (MeV)	0.59±0.08	2.34±0.16	4
Glitch length (pixel units)	8.5±0.5	8.8±0.5	1-2*
Total glitch rate (s^{-1})	0.83±0.12	0.045±0.026	0.002-0.35*

3.4. Discussion

The computed value for the average glitch length is in very good agreement with the expected value. This is quite obvious if we keep in mind that we assumed an isotropic shielding and an isotropic directional distribution for galactic incoming particles (see Sect. 2.3). But in the case of a less isotropic shielding distribution, these kind of simulations are very useful to determine glitch characteristics.

It would be interesting to compare the distributions of deposited energy generated by Monte-Carlo simulations with those derived directly from in-flight data. Unfortunately, a strong difficulty comes from the necessity of detecting glitches individually in the data. An advanced pattern recognition algorithm would be necessary to extract individually all glitches from the data, and then build their statistics.

Monte-Carlo simulation can be of great help in order to predict these distributions, and use them for optimization purposes. For example, this can have a major influence in the choice of materials in the immediate surroundings of the detector. More generally, simulated images of realistic particle effects allow to test various algorithms of glitch removal before the launch of the space experiment. It is easy to add some noise to simulated images in order to test the actual efficiency of algorithms. If one can be satisfied with the efficiency of removal algorithm on ground, on board removal can then be envisaged, rather than down-linking raw data and perform glitch removal on the ground. This can help to solve the problem of prohibitive huge data volume to be down-linked to the ground station.

4. GLITCH ESTIMATE FOR THE PACS BOLOMETERS ON BOARD HERSCHEL

4.1. Space environment for the satellite HERSCHEL

The HERSCHEL satellite is planned to be launched in 2007 by Ariane 5 launcher together with Planck or Eddington and to be put in a Lagrangian point 2 (L2) orbit at about 1.5×10^6 km from the Earth to the opposite side of the Sun. Although L2 is located about 4 times further than the Moon's orbit, this distance is quite negligible compared to the length scale of the cosmic ray intensity variation due to the solar magneto-sphere shielding. This allows to use the same model as ISOCAM in the cosmic ray intensity computation. However the HERSCHEL mission starts during a solar minimum activity period (maximum cosmic ray penetration) and may extend until a solar maximum activity (minimum cosmic ray penetration and maximum solar wind). This requires the whole range of particle intensities during the mission.

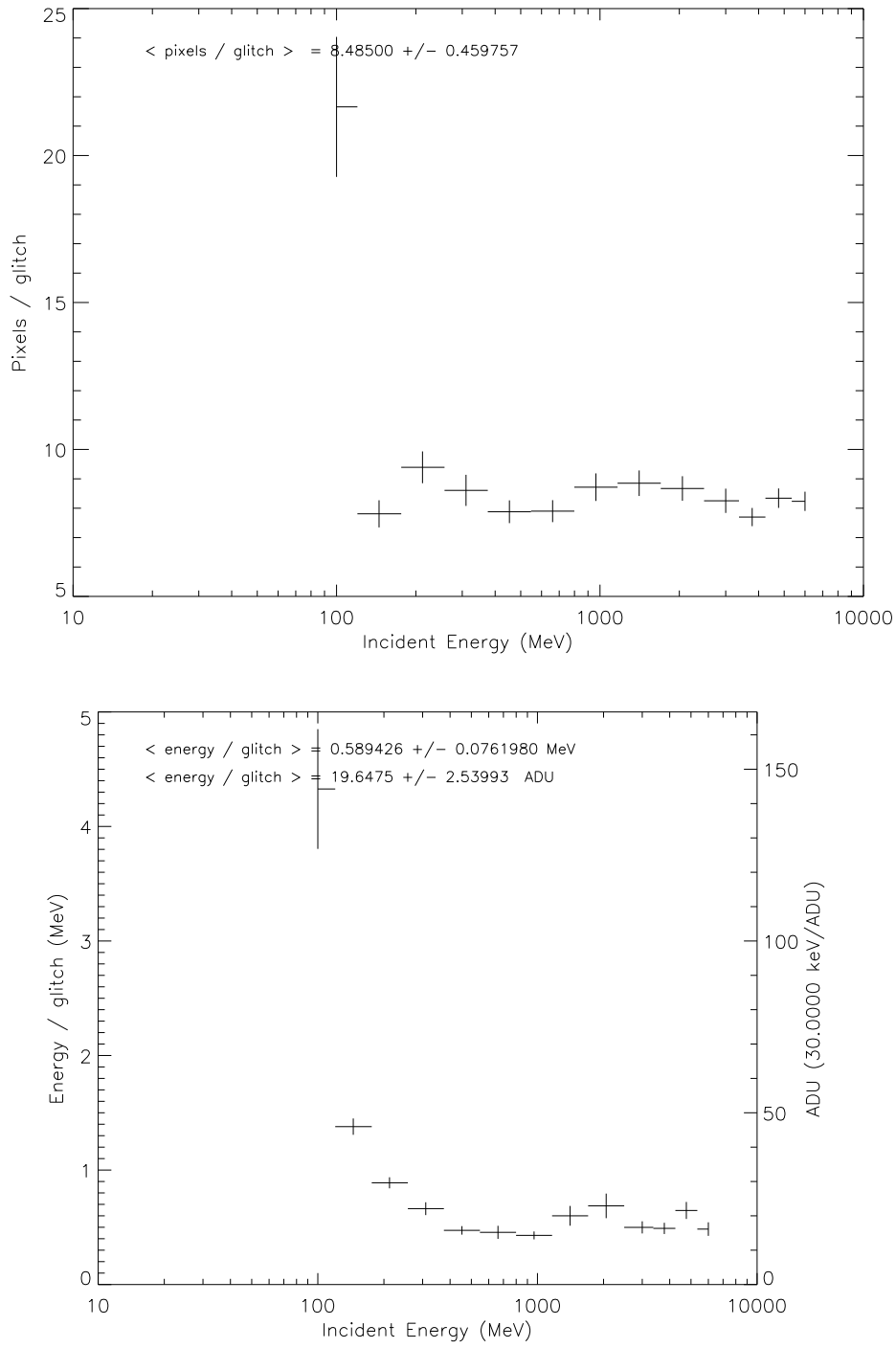

Figure 7. Spatial and temporal properties of glitches produced by galactic protons as a function of the energy of incident particle, computed by Monte-Carlo simulations. The glitch length is 8.5 ± 0.5 pixels for galactic protons and alphas which have both an isotropic directional distribution. The mean energy per glitch is 590 ± 80 KeV for protons and 2.34 ± 0.16 MeV for alphas.

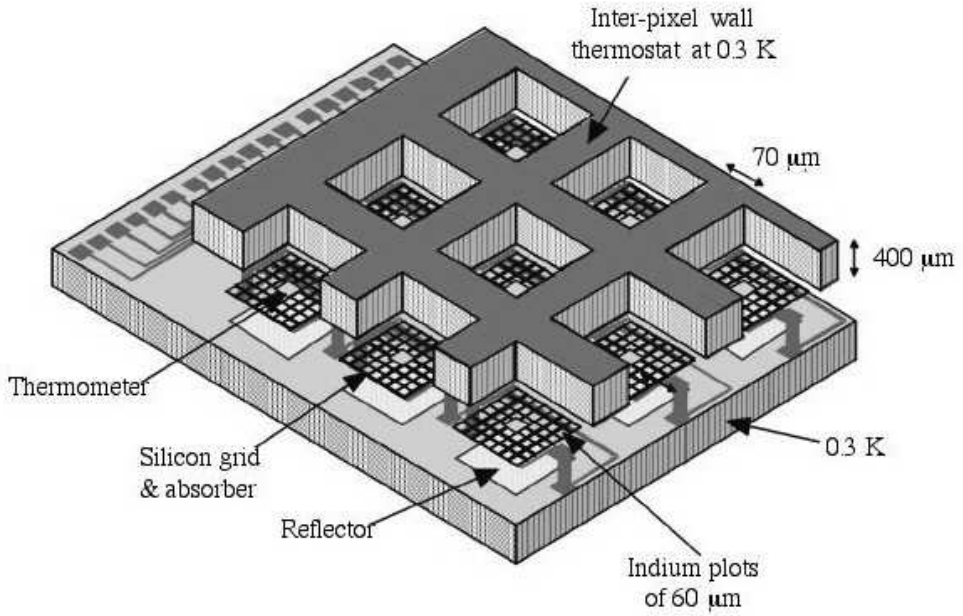

Figure 8. The structure of the PACS bolometers.

4.2. Geometry of the PACS bolometer

The PACS bolometers on board HERSCHEL has a geometrical structure as shown in Fig. 8. Two bolometer channels operate in parallel for a long (110 or 170 μm) and a short (75 μm) wavelengths. The absorber of each pixel is supported by a silicon grid of 5 μm thick together with a pixel-thermometer. Each pixel is suspended in a inter-pixel wall grid of 400 μm thick which carries also a reference-thermometer attached to it. This wall grid operates as a thermostat of the bolometer system.

The output signal is a function of the temperature difference between the pixel- and reference- thermometers. In the absence of any heating agent such as photons or particle hits the temperature difference is designed to be null.

Despite Fig. 8 does not show them, there are two columns of blind pixels which are heated to the mean temperature of the normal pixels. These pixels were added in order to suppress any undesired electronic temporal deviation by measuring the differential signals.

4.3. Glitch estimate in the bolometer data

Simple geometrical considerations on the volumes tells us that the probability for particles to hit the inter-pixel walls is approximately 10^4 times larger than for the pixel grids. The energy deposited by a particle impact in the inter-pixel walls raise their temperature for a while and then it goes back to the nominal temperature by the temperature regulation system. This process raise momentarily the temperature of the reference thermometers surrounding the impact of the particle. This produces negative glitches in the signals of the related pixels. Thus the number of negative glitches is about 10^4 times larger than that of positive glitches which are produced by a particle hitting the pixel grids.

The glitches on the blind pixels or their inter-pixel walls occur in the same way but these results in opposite sign in the pixels of a same row which are readout differentially with the affected blind pixel.

The thickness of the inter-pixel walls is 400 μm and the bolometer array is on a surface of about 12×12 mm (neglecting the blind pixels). Thus a large number (70.2%) of glitches affect only one pixel. The glitch length can be estimated approximately by simple geometrical considerations on the solid angle with respect to the

bolometer plane. Table 3 shows approximate percentages of glitch lengths computed in this way. Even if a particle hits only one inter-pixel wall, the glitch may appear in some nearest pixels because of the heat propagation. Further investigations are necessary to assess this effect.

Table 3. Negative glitch lengths on the PACS bolometer

Length (pixel units)	Solid angle (sr)	Percentage (%)
1	8.8	70.2
2	1.9	15.2
3	0.6	5.0
4	0.3	2.5
5	0.2	1.5
>16	0.2	1.8

The HERSCHEL telescope is passively cooled down to ≈ 80 K, because its active cooling is impossible due to its large size (3.5 m diameter for primary mirror). Therefore the chopping observation is most probably unavoidable. The glitch removal algorithm should work on each chopping time interval in order to avoid the false detection due to the sudden change of the flux level during the chopping. Following the investigations for ISOCAM, Monte Carlo simulations will be necessary for a better understanding of the glitches on the PACS bolometers.

5. CONCLUSION

The sensitivity of photodetector operated in space is limited by glitches caused by impacts of charged particles. For ISOCAM, the observed glitch rate was about 1 glitch/s outside the trapped radiation belts. The direct impact of GCRs represented about one third of this figure. The remainder came from secondary particles, mainly nuclear interaction particles and δ-rays. Glitch rates, as well as spatial and energetic properties of glitches, have been computed by Monte-Carlo simulations. They are in good agreement with both the measured and expected values. This simulation tool can be used in order to predict the effect of incoming particles on future space experiments.

ACKNOWLEDGMENTS

The authors would like to acknowledge Philippe Laurent for his help on the GEANT code.

REFERENCES

1. M. Kessler, J. Steinz, and M. A. et al., "The infrared space observatory (iso) mission," *Astronomy and Astrophysics* **315**, p. L27, 1996.
2. A. Heras, "Iso/first glitch working group final report," *ESA publication* **SAI/2001-013/Rp**, 2001.
3. C. Cesarsky, A. Abergel, and P. A. et al., "Isocam in flight," *Astronomy and Astrophysics* **315**, p. L32, 1996.
4. H. Dzitko, A. Claret, and J. Engelmann, "Cosmic ray effects on the isocam long wave detector," *Experimental Astronomy* **10**, pp. No. 2–3, 279–290, 2000.
5. A. Claret, H. Dzitko, and J. Engelmann, "Transient particle effects on the isocam instrument on-board the infrared space observatory," in *IEEE Trans. on Nucl. Sci.*, N. Conference, ed., *Vol.* **46**, pp. No. 6, 1511–1518, 1999.
6. CERN, *GEANT - Detector Description and Simulation Tool*, CERN Program Library Long Writeup W5013, CERN Geneva, Switzerland, 2000.